Utility of a Nonlinear Joint Dynamical Framework to Model a Pair of Coupled Cardiovascular Signals

Omid Sayadi, *Member, IEEE*, and Mohammad Bagher Shamsollahi, *Member, IEEE*

***Abstract*—We have recently proposed a correlated model to provide a Gaussian mixture representation of the cardiovascular signals, with promising results in identifying rhythm disturbances. The approach provides a transformation of the data into a set of integrable Gaussians distributed over time. Looking into the model from a new joint modeling perspective, it is capable of assembling a filtered estimation, and can be used to derive temporal information of the waveforms. In this paper, we present a step-by-step derivation of the joint model putting correlation assumptions together to conclude a minimal joint description for a pair of ECG–ABP signals. We then probe novel applications of this model, including Kalman filter based denoising and fiducial point detection. In particular, we use the joint model for denoising and employ the denoised signals for pulse transit time (PTT) estimation. We analyzed more than 70 h of data from 76 patients from the MIMIC database to illustrate the accuracy of the algorithm. We have found that this method can be effectively used for robust joint ECG–ABP noise suppression, with mean signal-to-noise ratio (SNR) improvement up to 23.2 (12.0) dB and weighted diagnostic distortion measures as low as 2.1 (3.3)% for artificial (real) noises, respectively. In addition, we have estimated the error distributions for QT interval, systolic and diastolic blood pressure before and after filtering to demonstrate the maximal preservation of morphological features (ΔQT: mean $\pm$ std $= 2.2 \pm 6.1$ ms; ΔSBP: mean $\pm$ std $= 2.3 \pm 1.9$ mmHg; ΔDBP: mean $\pm$ std $= 1.9 \pm 1.4$ mmHg). Finally, we have been able to present a systematic approach for robust PTT estimation ($r = 0.98, p < 0.001$, mean $\pm$ std of error $= -0.26 \pm 2.93$ ms). These findings may have important implications for reliable monitoring and estimation of clinically important features in clinical settings. In conclusion, the proposed framework opens the door to the possibility of deploying a hybrid system that integrates these algorithmic approaches for index estimation and filtering scenarios with high output SNRs and low distortion.**

***Index Terms*—Arterial blood pressure (ABP), electrocardiogram, extended Kalman filter, Gaussian mixture model (GMM), joint dynamical model, pulse transit time (PTT).**

I. Introduction

It is known that cardiovascular (CV) signals contain parameters of clinical significance and hold beat-to-beat variability which reflects the interaction between the disturbances on CV variables and the regulating system's response [1]. The pivotal role of neural mechanisms in CV pathophysiology has been postulated over the past few decades. Studies have shown that different physiological conditions and pathological disorders perturb the CV signals [2]. In the light of pre-existing studies [3]–[7] demonstrating the role of the autonomic nervous system (ANS) in the pathogenesis of CV diseases, the joint study of ECG, and specifically the heart rate variability (HRV), and arterial blood pressure (ABP) may hold promise as a method to assess the baroreceptor reflex sensitivity as a measure of the integrity of the ANS [3]. For this reason, the regulatory mechanisms that underlie CV beat-to-beat variability should be approached in a joint dynamic manner within the framework of the sympathovagal interactions that govern the instantaneous performance of the CV system [4], [5].

To date, ECG analysis is most commonly used as the first tool for initial screening and diagnosis of CV diseases in clinical setting. As a noninvasive and low-cost method, ECG provides valuable clinical information regarding the rate, timing, and regularity of the heart and, therefore, remains the benchmark method for cardiac arrhythmia detection [8]. However, commercial monitoring systems often include the capability to monitor several pressure signals, heart rate (HR), and the statistics of pressure waveforms, but few can reliably estimate components such as pulse pressure variation, pulse transit time (PTT), or signal quality measures [9].

Despite the success of statistic and dynamic modeling approaches toward ECG analysis, they have not been widely deployed to other CV signals, due to the unavailability of dynamic models for these signals. In a pioneering work, Clifford and McSharry [10], [11] proposed an artificial model for *generating* realistic ECG, ABP, and respiration signals using a Gaussian mixture model (GMM). The model included a respiratory signal to modulate the ECG amplitude and the high frequency of the pulse-to-pulse interval. A *statistical* model of CV signals was also proposed which used mixtures of sinusoidal functions to present some parameters of clinical interest relevant to ABP, pulse oximetry, and intracranial pressure [12]. Because of the statistical nature of the algorithm introduced in [12], neither the morphology information nor the joint interdependences of CV signals were taken into consideration in this model; therefore, the method could only track meaningful components of the CV signals based on an autoregressive formulation [12].

The concept of modeling coupled CV signals in a joint framework depends on the ability to formulate their timing and morphology, as well as their spatiotemporal relations. The aforementioned coupling which is present in any subset of the electromechanical cardiac signals occurs in the casual direction from

Manuscript received February 23, 2012; revised October 14, 2012 and January 14, 2013; accepted May 13, 2013. Date of publication May 17, 2013; date of current version June 27, 2013. This work was supported by the Departmental Research Assistant Scholarship #RA-86300384 granted by the School of Electrical Engineering, Sharif University of Technology, Tehran, Iran, and by a Research Award from the Exceptional Talents Center, Sharif University of Technology, Tehran, Iran.

O. Sayadi is with the Cardiovascular Research Center, Massachusetts General Hospital, Harvard Medical School, Charlestown, MA 02129 USA (e-mail: osayadi@ieee.org).

M. B. Shamsollahi is with the Biomedical Signal and Image Processing Laboratory, School of Electrical Engineering, Sharif University of Technology, Tehran 11365–9363, Iran (e-mail: mbshams@sharif.edu).

Digital Object Identifier 10.1109/JBHI.2013.2263836

the SA node, reflecting the correlation of the pressure signals with the HRV (mechanical path), while the coupling on the reverse casual direction is due to the baroreceptor response (baroreflex path). In either case, the electrical activity can be characterized as to be correlated to the pulsatile mechanical pressure signals, since they all originate from the same source. We have recently proposed a novel multidimensional generic model to provide adaptive estimations of the CV signals [13]. The estimations were used for polar phase analysis as well as instantaneous quality characterization for determining cardiac abnormalities. Furthermore, we have recently demonstrated the feasibility to model the temporal dynamics of coupled CV signals for realistic signal generation [14]. Following pioneering works of [15] and [16], in which the use of hidden Markov model (HMM) to sequence a series of GMM-based beat types were introduced, we proposed the use of a joint GMM representation together with an ergodic HMM for generating synthesized coupled CV signals with different beat types [14].

In this paper, we extend the joint modeling concept introduced in [14] to present a state-space model to be applied to coupled Bayesian estimation procedures. We provide a step-by-step model formulation and study the relation between temporal dependences and space dimension, in details. Our specific aims are summarized as follows.

1) *Aim1:* to validate a minimal order joint framework for Kalman filtering of a pair of CV signals (ECG and ABP).
2) *Aim2:* to propose a model-based algorithmic approach for robust estimation of PTT using the denoised estimations.

Unlike our recent work [13] where an N-dimensional joint model was introduced to obtain fidelity signals for abnormality verification, the model introduced in this paper is used for extended Kalman filter (EKF)-based joint tracking and temporal information estimation, which are two new applications of the joint framework. This paper is organized as follows. In Section II, we present the methods to construct the joint model, and explain its applications to denoising and PTT estimation. Study results are provided in Section III. Finally, discussion and conclusion are provided in Section IV.

II. Methods

In this section, the joint dynamical state-space model is introduced and our proposed algorithms for denoising and PTT estimation are explained in detail.

A. Model Design

As an early attempt toward dynamic modeling of the cardiac signals, McSharry *et al*. [17] introduced the electrographic dynamical model where a set of time-varying differential motion equations was used to generate a synthetic ECG signal. A semiperiodic circular limit cycle was used to account for the quasi-periodicity with an arbitrary number of basic functions at different turning points to reproduce the PQRST characteristic waveforms based on a GMM representation with amplitude α_i, angular spread b_i, and angular difference $\Delta\theta_i$, given by

$$\mathrm{GMM}(\alpha_i, b_i, \Delta\theta_i, k) = \sum_{i\in\{P,Q,R,S,T\}} \frac{\alpha_{i_k}}{b_{i_k}^2}\Delta\theta_i \exp\left(-\frac{\Delta\theta_{i_k}^2}{2b_{i_k}^2}\right) \tag{1}$$

where θ_i describes the angular PQRST peak locations and $\Delta\theta_{i_k} = (\varphi_k - \theta_{i_k}) \bmod (2\pi)$ with φ being the wrapped phase variable [18]. The polar equations of motion, discretized by sampling period, are given by two ordinary difference [19]

$$\begin{cases} \varphi_{k+1} = (\varphi_k + \omega_k\delta)\mathrm{mod}(2\pi) \\ s_{k+1} = s_k - \omega_k\delta\ \mathrm{GMM}\ (\alpha_i, b_i, \Delta\theta_i, k) + \eta_k \end{cases} \tag{2}$$

where ω is the beat-to-beat angular frequency of the RR interval, which is linearly related to the phase φ. The magnitudinal component of the dynamical system s represents the ECG signal with baseline perturbation η. Equation (2) can be viewed as a state-space formulation with state variables φ and s. As suggested in [19], an artificial phase ϕ may be assigned to the ECG observations to form the following observation equation:

$$\begin{cases} \phi_k = \varphi_k + u_{1_k} \\ z_k = s_k + u_{2_k} \end{cases} \tag{3}$$

where ϕ and z are the phase observation and the ECG measurement, respectively, and u_1 and u_2 are observation noises of the ECG in the phase and spatial domains.

An immediate extension of this model would be a realistic sketch for the dynamics of a coupled pair of CV signals that can track changes over time. The advantage of such an approach is that it can assemble a filtered version of the signals, and the filter outputs can be used to derive temporal information of the waveforms. Furthermore, the quality of the estimations can be used to obtain a confidence measure to identify rhythm changes [13], [20]. Without loss of generality, we assume ABP as the second paired CV signal to construct the model; however, the same approach may be applied to any other bandlimited CV signals with a quasi-periodic pattern originating from cardiac pulsation.

In order to procreate a joint formulation, we must translate the variables of interest into meaningful state variables, design appropriate state evolution function f and observation relation g to express the relationship between the observed signals $\underline{y}_k$ and states $\underline{x}_k$ in the form of

$$\begin{cases} \underline{x}_{k+1} = f(\underline{x}_k, \underline{w}_k, k) \\ \underline{y}_k = g(\underline{x}_k, \underline{v}_k, k) \end{cases} \tag{4}$$

and establish efficient relations between the parameters of the model to incorporate known physiologic variables. The details of this concept will be addressed next.

1) Combination Idea With Dimension Preservation: ECG signal is generated by electrical depolarization and repolarization of atria and ventricles, while ABP signal reflects mechanical interactions of contracting cardiac muscles with a vascular bed, and is characterized by a lower frequency content than the ECG. Although ECG and ABP are generated by different mechanisms, however, they are strictly coupled signals and the temporal *morphological* dynamics can be characterized using the same generic model with different parameters. Hence,

a straightforward extension of (2) would be to use the same set of dynamical equations with different GMM parameters for each individual CV signal. This approach designates two sets of equations with distinct parameters to each signal, and is capable of describing the process equations of paired signals in the form of a general diagonal state-space model with the following components:

$$\begin{aligned}
\underline{x}_k &= [\varphi_k^{\mathrm{ECG}} \;\; s_k^{\mathrm{ECG}} \;\; \varphi_k^{\mathrm{ABP}} \;\; s_k^{\mathrm{ABP}}]' \\
\underline{y}_k &= [\phi_k^{\mathrm{ECG}} \;\; z_k^{\mathrm{ECG}} \;\; \phi_k^{\mathrm{ABP}} \;\; z_k^{\mathrm{ABP}}]' \\
\underline{w}_k &= [\alpha_{i_k}^{\mathrm{ECG}}, b_{i_k}^{\mathrm{ECG}}, \theta_{i_k}^{\mathrm{ECG}}, \omega_k^{\mathrm{ECG}}, \eta_k^{\mathrm{ECG}}, \alpha_{i_k}^{\mathrm{ABP}}, \\
&\qquad b_{i_k}^{\mathrm{ABP}}, \theta_{i_k}^{\mathrm{ABP}}, \omega_k^{\mathrm{ABP}}, \eta_k^{\mathrm{ABP}}]' \\
\underline{v}_k &= [u_{1_k}^{\mathrm{ECG}} \;\; u_{2_k}^{\mathrm{ECG}} \;\; u_{1_k}^{\mathrm{ABP}} \;\; u_{2_k}^{\mathrm{ABP}}]' \qquad (5)
\end{aligned}$$

where $\underline{w}_k$ is the process noise vector with covariance matrix $Q = E\{(\underline{w}_k - \bar{\underline{w}}_k)(\underline{w}_k - \bar{\underline{w}}_k)'\}$ and $\underline{v}_k$ is the measurement noise vector with covariance matrix $R = E\{(\underline{v}_k - \bar{\underline{v}}_k)(\underline{v}_k - \bar{\underline{v}}_k)'\}$. The diagonal model has redundancy; therefore, we need to establish the correlation between the parameters of the model. This relationship can be endowed either with respect to the spatiotemporal locations of specific points in the signals, or even by considering the intrinsic consequential dependences of the signals. To devise a minimal order joint model, we present the following cases.

a) Equal angular frequency: The assumption of equal angular frequency for both ECG and ABP signals is valid if the HR affects the tachograms of these signals, equally [21]. This is generally true due to the same time-point-based modulations of the pulse wave velocity and of the cardiac contractility. Assuming $\omega^{\mathrm{ECG}} = \omega^{\mathrm{ABP}}$, the state-space equations remain unchanged, while the process noise vector reduces to $\underline{w}_k = [\alpha_{i_k}^{\mathrm{ECG}}, b_{i_k}^{\mathrm{ECG}}, \theta_{i_k}^{\mathrm{ECG}}, \eta_k^{\mathrm{ECG}}, \alpha_{i_k}^{\mathrm{ABP}}, b_{i_k}^{\mathrm{ABP}}, \theta_{i_k}^{\mathrm{ABP}}, \eta_k^{\mathrm{ABP}}, \omega_k]'$.

b) Identical Gaussian kernel locations: Mathematically speaking, it is possible to model an individual CV signal using a finite number of Gaussian kernels. In fact, a GMM representation can effectively model the ECG signal, and if applied with different amplitudes and spreads but with the same locations ($\theta_i^{\mathrm{ECG}} = \theta_i^{\mathrm{ABP}}, i \in \{P, Q, R, S, T\}$), it can also provide a good fit for an ABP signal. This assumption keeps the state-space equations unchanged, while the process noise vector reduces to $\underline{w}_k = [\alpha_{i_k}^{\mathrm{ECG}}, b_{i_k}^{\mathrm{ECG}}, \omega_k^{\mathrm{ECG}}, \eta_k^{\mathrm{ECG}}, \alpha_{i_k}^{\mathrm{ABP}}, b_{i_k}^{\mathrm{ABP}}, \omega_k^{\mathrm{ABP}}, \eta_k^{\mathrm{ABP}}, \theta_{i_k}]'$. However, since the angular locations of both the ECG and ABP Gaussian kernels are process noise components (5), their corresponding values would not be estimated during the filtering procedure. Accordingly, we can keep the process noise vector unchanged, and instead assume the same covariance values for all angular locations.

2) Combination Idea With Dimension Reduction: The previously described approach toward joint modeling was based on relating the process noise parameters which imposed no changes to the state variables and hence preserved the space dimension. However, a more accurate approach is to find relations between the state variables to obtain a coupled state-space model with reduced dimension.

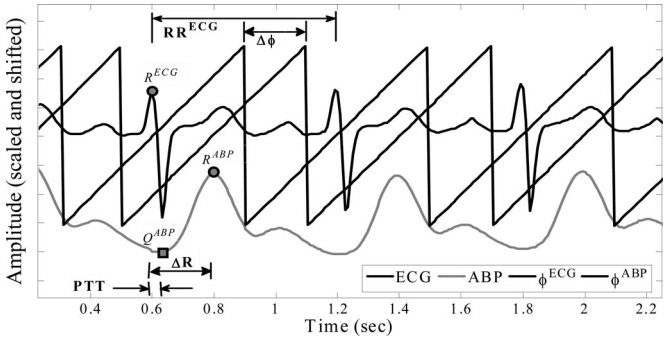

Fig. 1. Representative example of real paired ECG (solid black) and ABP (solid gray) records, with the corresponding artificial wrapped phase signals (ϕ^{ECG}: dashed, ϕ^{ABP}: dotted). The first R peaks for ECG and ABP signals are shown with a filled circle. RR interval for the ECG signal as well as the temporal lag (for both ΔR and $\Delta\phi$) is shown with double-sided arrows.

Each heartbeat is initiated by a rhythmic pacemaker within the heart and is conducted throughout the organ to produce a coordinated contraction. The effect of the electrical impulse is first seen on the ECG signal, and after a specific delay, is observed in the ABP signal [2], [5]. Accordingly, the timing of these signals could be controlled by a single cycle (referenced to ECG and delayed for ABP). On the other hand, and as per stationary and often sedated conditions of patients in a clinical setting, the HRs remain quasi-periodic signals with slowly varying amplitudes, morphologies, and even fundamental frequencies. This opens the door to the possibility of modeling the pseudo-periodic behavior of the cardiac dipole as it evolves during the cardiac cycle [19], [22].

To embed the periodicity information of both coupled signals into a single phase variable, we proposed a phase relationship between the corresponding state variables of the ECG and ABP signals [14]. We had visually observed that the RR tachogram of ABP signal is a shifted variant of its ECG counterpart, due to the physiological delay in the occurrences of $\mathrm{R}^{\mathrm{ECG}}$ and $\mathrm{R}^{\mathrm{ABP}}$. Hence, it is possible to translate the shift between $\mathrm{R}^{\mathrm{ECG}}$ and $\mathrm{R}^{\mathrm{ABP}}$ into a dynamic lag which relates the corresponding phase parameters of ECG and ABP signals. This idea is demonstrated in Fig. 1 where the phase delay, $\Delta\phi$, is equal to the angular distance between the R peaks of the signals, ΔR. The reason is because each phase observation signal is referenced to its corresponding R peak. Accordingly, the phase variables can effectively be related as

$$\varphi_k^{\mathrm{ABP}} = \varphi_k^{\mathrm{ECG}} - \Delta\theta_{R_k} \qquad (6)$$

where $\Delta\theta_{R_k} = \theta_{R_k}^{\mathrm{ABP}} - \theta_{R_k}^{\mathrm{ECG}}$ (see Fig. 1). It is worth noting that ΔR is an adaptive term which dynamically changes over time due the HRV [23]. Since the artificial wrapped phase signals are referenced to the corresponding R peak, $\theta_{R_k}^{\mathrm{ECG}}$ may therefore point to a zero crossing for the ECG phase signal [19], as shown in Fig. 1. Substituting $\theta_{R_k}^{\mathrm{ECG}} = 0$ in (6) yields the following fundamental inter-dependence

$$\varphi_k^{\mathrm{ABP}} = \varphi_k^{\mathrm{ECG}} - \theta_{R_k}^{\mathrm{ABP}} \qquad (7)$$

Equation (7) provides one possible explanation for the delayed patterns of coupled ECG–ABP pairs, based on which the

timing and rates of the signal components are controlled by one phase variable and the second phase variable becomes redundant. However, the second and fourth state variables which accounts for the morphology changes of the signals remain unchanged. Although the phase interaction (7) does not cover the full range of correlations between CV signals, it is sufficient to define a minimal joint representation to relate the time cycle of the pulsatile events in ECG and ABP.

In accordance with the proposed idea in Section II-A1b, it is possible to assign the same covariance values to the angular locations of the GMM kernels, i.e., θ_i^{ECG} and θ_i^{ABP}. By substituting (7) in the diagonal model and excluding the redundant ABP phase variable, the correlated joint dynamical state-space representation with reduced number of state variables and noise parameters is given by

Process equation:

$$\begin{cases} \varphi_{k+1}^{\mathrm{ECG}} = (\varphi_k^{\mathrm{ECG}} + \omega_k \delta) \mathrm{mod}(2\pi) \\ s_{k+1}^{\mathrm{ECG}} = s_k^{\mathrm{ECG}} - \omega_k \delta \ \mathrm{GMM}\ (\alpha_i^{\mathrm{ECG}}, b_i^{\mathrm{ECG}}, \Delta\theta_i^{\mathrm{ECG}}, k) + \eta_k^{\mathrm{ECG}} \\ s_{k+1}^{\mathrm{ABP}} = s_k^{\mathrm{ABP}} - \omega_k \delta \ \mathrm{GMM}\ (\alpha_i^{\mathrm{ABP}}, b_i^{\mathrm{ABP}}, \Delta\theta_i^{\mathrm{ABP}}, k) + \eta_k^{\mathrm{ABP}} \end{cases} \tag{8}$$

Observation equation:

$$\begin{cases} \phi_k^{\mathrm{ECG}} = \varphi_k^{\mathrm{ECG}} + u_{1_k}^{\mathrm{ECG}} \\ z_k^{\mathrm{ECG}} = s_k^{\mathrm{ECG}} + u_{2_k}^{\mathrm{ECG}} \\ z_k^{\mathrm{ABP}} = s_k^{\mathrm{ABP}} + u_{2_k}^{\mathrm{ABP}} \end{cases} \tag{9}$$

where

$$\begin{aligned} \Delta\theta_{i_k}^{\mathrm{ECG}} &= (\varphi_k^{\mathrm{ECG}} - \theta_{i_k}^{\mathrm{ECG}}) \bmod (2\pi) \\ \Delta\theta_{i_k}^{\mathrm{ABP}} &= (\varphi_k^{\mathrm{ABP}} - \theta_{i_k}^{\mathrm{ABP}}) \bmod (2\pi). \end{aligned} \tag{10}$$

In order to exclude the redundant ABP phase variable, we use the correlative interdependence of ECG–ABP pairs introduced in (7). Substituting (7) into (10) simplifies the angular differences to

$$\begin{aligned} \Delta\theta_{i_k}^{\mathrm{ECG}} &= (\varphi_k^{\mathrm{ECG}} - \theta_{i_k}^{\mathrm{ECG}}) \bmod (2\pi) \\ \Delta\theta_{i_k}^{\mathrm{ABP}} &= (\varphi_k^{\mathrm{ECG}} - \theta_{i_k}^{\mathrm{ABP}} - \theta_{R_k}^{\mathrm{ABP}}) \bmod (2\pi). \end{aligned} \tag{11}$$

The proposed joint state-space model, (8) and (9), may be described as a discrete map, where the quasi-periodic evolution of the cardiac cycle is reflected by the movement of the trajectories around the attracting limit cycle in phase plane, while the interbeat variation is reproduced using its motion in terms of GMM parameters. These two basic components, i.e., amplitude and phase, are the essential variables of a dynamic state space to describe the temporal characteristics of correlated CV signals. The vector components of the new model are redefined as

$$\begin{aligned} \underline{x}_k &= [\varphi_k^{\mathrm{ECG}} \ \ s_k^{\mathrm{ECG}} \ \ s_k^{\mathrm{ABP}}]' \\ \underline{y}_k &= [\phi_k^{\mathrm{ECG}} \ \ z_k^{\mathrm{ECG}} \ \ z_k^{\mathrm{ABP}}]' \\ \underline{w}_k &= [\alpha_{i_k}^{\mathrm{ECG}}, b_{i_k}^{\mathrm{ECG}}, \theta_{i_k}^{\mathrm{ECG}}, \alpha_{i_k}^{\mathrm{ABP}}, b_{i_k}^{\mathrm{ABP}}, \theta_{i_k}^{\mathrm{ABP}}, \\ &\quad \eta_k^{\mathrm{ECG}}, \eta_k^{\mathrm{ABP}}, \omega_k]' \\ \underline{v}_k &= [u_{1_k}^{\mathrm{ECG}} \ \ u_{2_k}^{\mathrm{ECG}} \ \ u_{2_k}^{\mathrm{ABP}}]'. \end{aligned} \tag{12}$$

B. Denoising

The CV records of the biopotentials associated with the contractions of the heart muscle provide useful information for the detection, diagnosis, and treatment of cardiac and CV diseases. However, these signals are usually corrupted with unwanted interference, generally referred to as noise or artifact. Since the interference is often inband, time-coincident, or similar to cardiac activity, accurate information extraction requires effective characterization of the constituent waveform morphologies [24]. In general, the correct choice of the filtering technique depends not only on the temporal and spectral characteristics of the noise and signal, but also on the application. Having proposed a state-space formulation and as an attempt to estimate the hidden state of this system using the set of observation time series, the state-space model-based Bayesian filtering approach and in particular, the Kalman filter may therefore serve as an efficient denoising technique. We use the EKF as an extension of the traditional Kalman filter that can be applied to a nonlinear model (8) [25]. In order to employ the EKF, the nonlinear equations of motion must be linearized with respect to the state variables and the noise variables [26]. By defining

$$\begin{cases} \varphi_{k+1}^{\mathrm{ECG}} = F_0(\varphi_k^{\mathrm{ECG}}, \omega_k, k) \\ s_{k+1}^{\mathrm{ECG}} = F_1(s_k^{\mathrm{ECG}}, \varphi_k^{\mathrm{ECG}}, \omega_k, \alpha_i^{\mathrm{ECG}}, b_i^{\mathrm{ECG}}, \theta_i^{\mathrm{ECG}}, \eta_k^{\mathrm{ECG}}, k) \\ s_{k+1}^{\mathrm{ABP}} = F_2(s_k^{\mathrm{ABP}}, \varphi_k^{\mathrm{ECG}}, \omega_k, \alpha_i^{\mathrm{ABP}}, b_i^{\mathrm{ABP}}, \theta_i^{\mathrm{ABP}}, \eta_k^{\mathrm{ABP}}, k) \end{cases} \tag{13}$$

the linearized model with respect to the process components may be expressed as

$$\begin{aligned} &\frac{\partial F_0}{\partial \omega} = \delta \quad \frac{\partial F_1}{\partial \eta_i^{\mathrm{ECG}}} = \frac{\partial F_2}{\partial \eta_i^{\mathrm{ABP}}} = 1 \\ &\frac{\partial F_0}{\partial \alpha_i^j} = \frac{\partial F_0}{\partial b_i^j} = \frac{\partial F_0}{\partial \theta_i^j} = \frac{\partial F_0}{\partial \eta_i^j} = 0 \quad j \in \{\mathrm{ECG}, \mathrm{ABP}\} \\ &\frac{\partial F_\ell}{\partial \omega} = -\delta \ \mathrm{GMM}\ (\alpha_i^j, b_i^j, \Delta\theta_i^j, k) \\ &\frac{\partial F_\ell}{\partial \alpha_i^j} = -\delta\, \omega_k \frac{\Delta\theta_i^j}{(b_i^j)^2} \exp\left(-\frac{1}{2}(\frac{\Delta\theta_i^j}{b_i^j})^2\right) \\ &\frac{\partial F_\ell}{\partial b_i^j} = 2\delta\, \omega_k \frac{\alpha_i^j \Delta\theta_i^j}{(b_i^j)^3} \left(1 - \frac{1}{2}(\frac{\Delta\theta_i^j}{b_i^j})^2\right) \exp\left(-\frac{1}{2}(\frac{\Delta\theta_i^j}{b_i^j})^2\right) \\ &\frac{\partial F_\ell}{\partial \theta_i^j} = \delta\, \omega_k \frac{\alpha_i^j}{(b_i^j)^2} \left(1 - \left(\frac{\Delta\theta_i^j}{b_i^j}\right)^2\right) \exp\left(-\frac{1}{2}\left(\frac{\Delta\theta_i^j}{b_i^j}\right)^2\right) \end{aligned} \tag{14}$$

where $\ell = 1$ for $j = \mathrm{ECG}$ and $\ell = 2$ for $j = \mathrm{ABP}$. The linearization of (8) with respect to the state variables yields

$$\begin{aligned} &\frac{\partial F_0}{\partial s_k^{\mathrm{ECG}}} = \frac{\partial F_0}{\partial s_k^{\mathrm{ABP}}} = 0 \quad \frac{\partial F_0}{\partial \varphi_k^{\mathrm{ECG}}} = \frac{\partial F_1}{\partial s_k^{\mathrm{ECG}}} = \frac{\partial F_2}{\partial s_k^{\mathrm{ABP}}} = 1 \\ &\frac{\partial F_\ell}{\partial \varphi_k^j} = -\delta\omega_k \ \mathrm{GMM}\left(\alpha_i^j \left(1 - \left(\frac{\Delta\theta_i^j}{b_i^j}\right)^2\right), b_i^j, \Delta\theta_i^j, k\right). \end{aligned} \tag{15}$$

Having formed the nonlinear formulation (8) with the derived linearized model (14) and (15), the time propagation and the measurement propagation equations of the joint EKF (JEKF) may be applied to obtain the state estimations $\hat{s}^{\mathrm{ECG}}$ and $\hat{s}^{\mathrm{ABP}}$, which are regarded as the denoised version of the input signals [26], [27]. To improve the filtering performance, it is also possible to use the information of future observations in the estimation procedure to give better estimates of the current state, resulting in a joint extended Kalman smoother (JEKS). Further details regarding the model-based Kalman filtering may be found in [13], [19], and [20].

C. CV Signal Segmentation and PTT Estimation

Since we have a joint model, a related application domain would be to extract the concurrent feature location and segmentation of ECG-ABP signals using the EKF estimations.

As an extension of previous works on ECG segmentation [28]–[31], Gaussian descriptors may be used to locate the characteristic points of paired ECG–ABP records, since they explicitly describe the amplitude a_i, width b_i, and location θ_i of each point in the ECG and ABP waveforms. However, this would require defining a new model with additional state variables. To utilize the previously introduced minimal order model (see Section II-A1), we propose an alternate approach to employ the JEKF estimation for point detection. The following application example demonstrates how well the JEKF can track the parameters of interest, such as PTT, using the denoised estimations.

As a popular arterial stiffness marker, PTT is inversely related to the pulse wave velocity down the artery which is known to be influenced by ABP, HR, arterial compliance, and hence age [32]. PTT has potential clinical use in measurement of respiratory effort, as well as detection of microarousals [33]. Since the 1990s, it has been used to measure sympathetic activation during upper airway obstruction in sleep [33]. Over the past few years, there seems general consensus in the notion that PTT reflects sympathetic tone. Some studies reported that PTT changes with anesthetic depth [34], [35], while some others suggest that PTT reflects autonomic tone and may function as a surrogate marker of ABP [35], [36]. Furthermore, PTT has shown to respond to nociceptive stimulation independently of HR [35]. Most recently, PTT has been used as a marker of changes in sympathetic vasoconstriction and a quick predictor of axillary brachial plexus block [37].

It is generally accepted that as ABP falls, tension in the arterial wall falls and the PTT increases, and vice versa. The systolic (peak) ABP has therefore been linearly coupled to the mean HR, and hence inversely to the PTT [38]. PTT is proportional to the time between the peak of the QRS complex of the ECG signal and the start of the reflected dominant wave in ABP signal (points $\mathrm{R}_{\mathrm{ECG}}$ and $\mathrm{Q}_{\mathrm{ABP}}$ in Fig. 1). Following [10], we define

$$\mathrm{PTT} = 2\pi/(\theta_Q^{\mathrm{ABP}} - \theta_R^{\mathrm{ECG}}). \tag{16}$$

One way to have an estimate of the angular locations $\hat{\theta}_Q^{\mathrm{ABP}}$ and $\hat{\theta}_R^{\mathrm{ECG}}$ is to use our previously developed concept [30] to incorporate autoregressive dynamics for the process noise components. Alternatively, we propose to use the phase information of the correlated ECG–ABP pair, as provided by the estimated phase signal $\hat{\varphi}_K^{\mathrm{ECG}}$. Since $\mathrm{R}_{\mathrm{ECG}}$ is assumed to be located at $\theta_R = 0$ during the phase signal construction, the preceding waves (P and Q) and the proceeding waves (S and T) will occur in the range of $[-\pi, 0]$ and $[0, +\pi]$, respectively. Consequently, $\mathrm{R}_{\mathrm{ECG}}$ will be located by zero crossing detection of the estimated phase signal $\hat{\varphi}_k^{\mathrm{ECG}}$. Moreover, the location of $\mathrm{Q}_{\mathrm{ABP}}$ will be determined by a max-min search of the ABP wrapped-phase in the range of $[-\pi, 0]$. However, since the ABP phase is related to the ECG phase according to (7), it is possible to perform a max-min search for the estimated ECG wrapped-phase $\hat{\varphi}_k^{\mathrm{ECG}}$, in the range of $[0, +\pi]$, and assign the first detected point to the $\mathrm{Q}_{\mathrm{ABP}}$. The proposed PTT estimation procedure is summarized in Fig. 2. It should also be noted that to have an explicit model of PTT, elaborate explicit delays should have been built into the system to account for the electromechanical delay between the occurrence of R-wave on ECG and the opening of the aortic valve. This delay, often referred to as the left ventricular isometric contraction time, may be considered by incorporating the pre-ejection period and the ejection time [10].

III. Results

In this section, the versatility and utility of our proposed framework for the joint processing of ECG–ABP pair are demonstrated. The Kalman estimator is used for noise suppression and correlated features extraction. The proposed algorithm was implemented in MATLAB and was tested on a 2.67-GHz Core i7 machine. For performance evaluation, we have used the MIMIC database [39], [40], which is a collection of multiparameter recordings of ICU patients and the MIT-BIH noise stress test database [40], [41].

A. Kalman-Based Joint Filtering of ECG and ABP Signals

Fig. 3 presents a qualitative demonstration of model-based noise reduction in the presence of different types of artifacts including white and real noises. We see that the joint EKF estimations have admirably tracked the clean signal morphology, even in rather low input signal-to-noise ratio (SNR). In Fig. 3(a), we show the potential success of JEKF to eliminate artificial white noise, while preserving the morphology of both signals. In clinical settings, the electrical activity due to muscle contractions (with frequencies ranging between dc and 10 kHz with an average amplitude of 10% of full-scale deflection) as well as patient–electrode motion artifacts are the most common contaminations to CV recordings, which cannot be removed easily by simple bandpass filters [24], [42]. In Fig. 3(b) and (c), we show that the proposed JEKF scheme is also able to suppress these two types of artifacts, while preserving diagnostic morphological information of the signals. In fact, the underlying dynamics for the ECG–ABP signals constrain the filtering to be within an envelope of the adaptive template morphology, avoiding muscle and motion artifact to affect the denoised signal (see the difference in T wave offsets, PQ, QT, and ST intervals).

For quantitative performance evaluation, we have implemented the proposed JEKF and JEKS methods, together with the following benchmark algorithms.

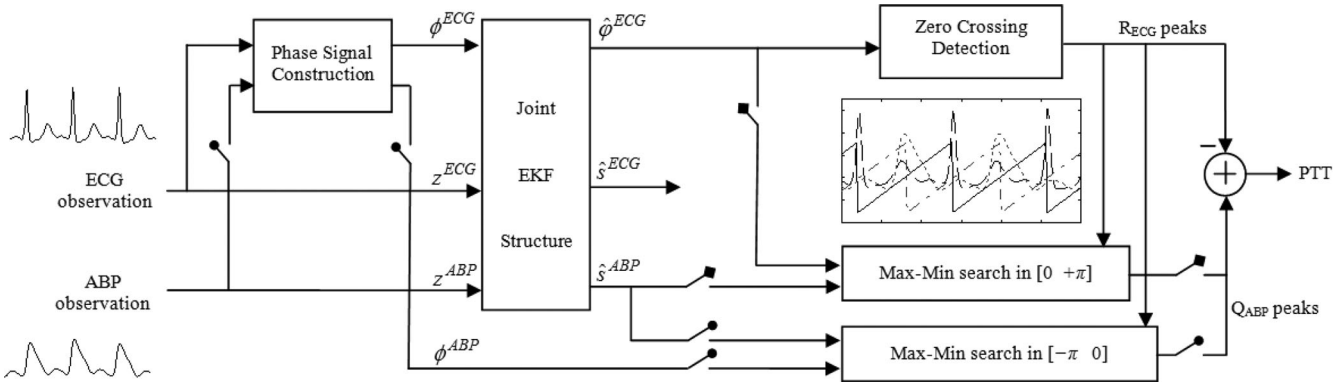

Fig. 2. General block diagram of the proposed denoising and PTT estimation algorithm based on the joint EKF structure: (a) using the ABP phase signal (when ↖ switches are closed (b) without using the ABP phase signal (when ↗ switches are closed).

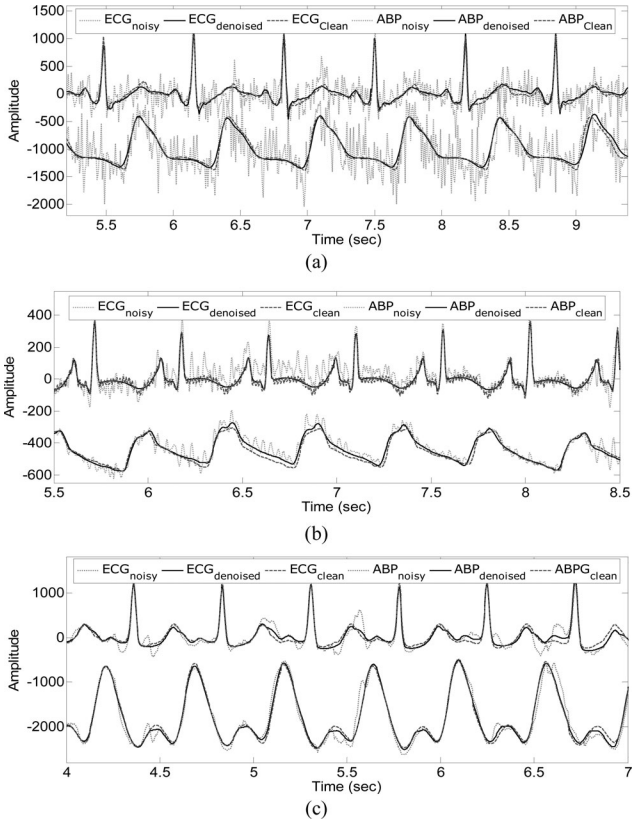

Fig. 3. Demonstration of model-based noise reduction for different types of input noises using JEKF. (a) Record 211 with an additive white Gaussian noise of −2 dB. (b) Record mgh003 with calibrated amount of real EMG noise (input SNR of 1 dB for the noisy portion). (c) Record 39 with real motion artifacts (input SNR of 6.7 dB). (solid: clean signal, dashed: denoised signal, gray: noisy signal). Note that the amplitudes on the y-axis are scaled and shifted.

1) *WT:* The conventional wavelet transform with the best previously reported configuration (6) levels of decomposition using Coiflets3 mother wavelet and deploying the Stein's unbiased risk estimate shrinkage rule, together with a single-level rescaling and a soft thresholding strategy, as was tested by Sameni *et al*. [19].
2) *EKF2:* The EKF with two state variables (2) and separate conventional dynamic models for ECG and ABP [19].
3) *EKS2:* The extended Kalman smoother with two state variables (2) and separate conventional dynamic models for ECG and ABP [19].
4) *EKF17:* The parameter-based EKF with 17 state variables, including the two state variables (2) and 15 autoregressive dynamics for Gaussian parameters [43], [44].

The MIMIC database [39] was used for performance evaluation. From the total 121 subjects, we selected those with at least one surface ECG lead, together with a recorded ABP signal. We then exclude the cardiogenic shock patients, narrowing down the subjects to 76 individuals, for which the last 1 h recordings were visually inspected by an experienced cardiologist to extract clean data segments. Real ECG artifacts were chosen from the noise stress test database [41] and realistic ABP noises were simulated using both the high-frequency components of the ECG motion artifacts and Brownian motion, as proposed in [45]. Calibrated amount of real noises, white noise, and colored noises (pink and brown) were added to the coupled ECG-ABP segments, and the noisy signals were presented to the mentioned filters. To ensure the consistency of the results, for every method, the whole procedure was repeated 50 times; each time using a different set of random noise at the input, and the signal-to-noise ratios of the denoised signals were calculated over the second half of the filtered segments, to make sure that the transient effects of the filters would not influence the SNR calculations. We estimate the SNR improvement for ECG signal (to measure amplitude errors) and also over ST segment (to quantify ST level distortion). Additionally, to verify how well the clinical features (location, duration, amplitudes, and shapes) of the signals are preserved after filtering, we have estimated the weighted diagnostic distortion (WDD) [46] with the same features and penalty matrices as described in [46] and a similar diagonal matrix of weights to the one defined in [43]. In Table I, we report the WDD as well as the mean paired SNR improvement for ECG and ABP for different input SNRs and for all filtering methods. The results show that the filter performance increases as the input SNR decreases from + 6 dB to −6 dB, while the magnitude and slope of increase is larger for the proposed joint algorithms. We observed that the ST improvement for JEKF and JEKS is in the same range with the signal improvement, describing the ability of the filter

TABLE I
PERFORMANCE COMPARISON (SNR IMPROVEMENT, WDD, AND RUN TIME) OF BENCHMARK METHODS TO THE PROPOSED JOINT MODEL-BASED METHOD FOR COUPLED ECG–ABP FILTERING

Noise Type	Input SNR (dB)	Method																	
		WT			EKF2			EKS2			EKF17			JEKF			JEKS		
		ECG SNR_{imp} (dB)	ST SNR_{imp} (dB)	WDD (%)	ECG SNR_{imp} (dB)	ST SNR_{imp} (dB)	WDD (%)	ECG SNR_{imp} (dB)	ST SNR_{imp} (dB)	WDD (%)	ECG SNR_{imp} (dB)	ST SNR_{imp} (dB)	WDD (%)	ECG SNR_{imp} (dB)	ST SNR_{imp} (dB)	WDD (%)	ECG SNR_{imp} (dB)	ST SNR_{imp} (dB)	WDD (%)
White	− 6	20.28	17.09	8.3	21.06	20.33	4.3	21.65	21.44	4.1	22.36	21.11	5.0	23.19	23.03	2.9	22.07	21.90	2.9
	0	16.08	14.11	6.6	16.98	15.50	3.5	17.04	15.90	3.4	17.90	16.06	3.7	18.55	18.04	2.9	19.11	19.05	2.8
	+ 6	15.48	13.33	6.1	15.35	14.01	3.4	15.13	14.19	3.0	16.19	15.19	3.6	16.67	16.26	2.5	14.94	14.44	2.1
Pink	− 6	15.38	13.41	9.1	15.74	14.11	6.7	15.23	14.00	6.0	16.37	15.69	6.1	17.22	17.11	3.2	17.12	17.21	3.0
	0	12.12	10.00	9.0	12.00	10.60	5.6	12.71	11.18	5.5	13.44	12.17	5.2	15.00	14.70	3.1	15.66	15.16	3.1
	+ 6	9.57	7.99	7.8	10.48	8.92	4.0	11.22	10.03	3.6	12.80	11.17	4.1	13.11	12.73	3.0	13.01	13.00	3.0
Brown	− 6	10.48	8.01	8.8	12.45	10.33	6.1	13.96	12.12	6.0	14.00	12.20	5.8	14.53	14.00	3.5	16.42	16.19	3.2
	0	9.11	7.91	8.3	10.61	9.11	5.2	10.06	9.20	5.0	11.15	9.90	4.7	13.75	13.11	3.2	13.45	13.55	3.0
	+ 6	7.83	6.10	7.3	9.67	8.20	4.2	9.46	8.31	4.5	10.44	9.55	3.8	11.57	11.09	3.0	10.88	10.17	2.9
Real	− 6	7.21	4.00	15.9	11.15	9.10	8.5	11.98	10.10	8.1	11.38	10.31	8.5	10.97	10.95	4.8	12.00	12.63	4.1
	0	7.19	4.12	13.5	10.83	9.09	6.1	10.93	9.50	5.2	9.66	8.20	5.2	10.00	9.92	4.3	11.50	11.89	4.0
	+ 6	7.23	4.02	12.1	7.61	6.13	5.0	7.97	6.85	4.5	8.24	6.66	5.0	8.40	8.68	3.5	9.21	9.09	3.3
Run time (s)		0.20			5.93			6.82			9.13			4.74			5.52		

to preserve low amplitude components. We also noticed that the joint methods provide a lower distortion rate (JEKF max distortion: 4.8% for real noises and 3.5% for artificial noises; JEKS max distortion: 4.1% for real noises and 3.2% for artificial noises), making JEKF and JEKS superior to the other methods being tested. Furthermore, the time complexity evaluation of the algorithms (the actual run time for a 1 min signal) reveals that the joint model structure has the second least run time, because of its joint relations and the reduced dimension.

In order to systematically analyze the effect of a filter on the ECG and ABP signals in terms of useful clinical metrics, we estimated the QT interval for ECG, and the systolic blood pressure (SBP) and diastolic blood pressure (DBP) for ABP over all input SNRs. In order to investigate the accuracy of the joint filtering method with real clinical parameters, 30 patient records were extracted from the MIMIC database, yielding more than 2 h of data with approximately 8500 beats. Due to the significant changes in ABP signals and pressure ranges, we did not use the following categories of patients: sepsis, bleeding, coma, angina, cardio shock, cardiac heart failure, and post operation. From the remaining 21 patients (some subjects have contributed more than one recording), we extracted variable length ECG–ABP signals of about 10 min from the last part of each recording, to ensure that the patient has been in ICU for more than 24 h and the measurements reflect the stable phase of the patient monitoring. The signals were presented to all filtering methods and the outputs of the filters were analyzed for the determination of QT, SBP, and DBP indices. For implementing the QT interval extraction, we have used the QRS detection algorithm [47] and T wave detection method of [48]. The SBP and DBP were estimated using a simple max/min search during each cardiac cycle.

Box plots for ΔQT, ΔSBP, and ΔDBP for all methods are shown in Fig. 4, where the delta represents the difference between clean and filtered signals. It can be observed that the joint

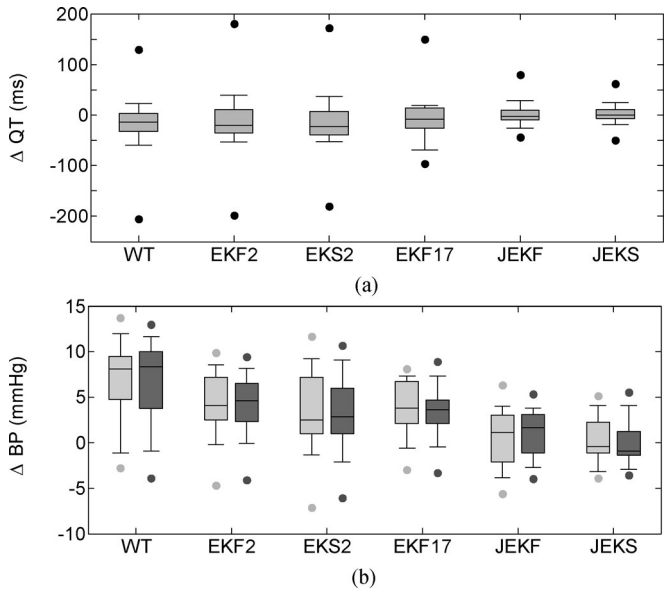

Fig. 4. Performance comparison of different filtering schemes for (a) ΔQT interval and (b) ΔSBP (light gray) and ΔDBP (dark gray) measurements (Δ is defined as the difference between the clean and filtered signals). Box plot representation of the error distributions is shown for all filtering methods. In each figure, the box indicates the median value with 90–10% percentiles, error bars show 95–5% percentiles, and max/min values are shown by circles.

methods (JEKF and JEKS) have the best performance in QT detection (ΔQT: mean $\pm$ std $= 2.2 \pm 6.1$ ms, median < 3 ms, 90–10% percentile < 12 ms, 95–5% percentile < 30 ms), as well as in the estimation of blood pressure components (ΔSBP: mean $\pm$ std $= 2.3 \pm 1.9$ mmHg, median < 2 mmHg, 90–10% percentile < 4 mmHg, 95–5% percentile < 5 mmHg, ΔDBP: mean $\pm$ std $= 1.9 \pm 1.4$ mmHg, median < 2 mmHg, 90–10% percentile < 3 mmHg, 95–5% percentile < 5 mmHg). Moreover, compared to other filtering methods, the variations of the

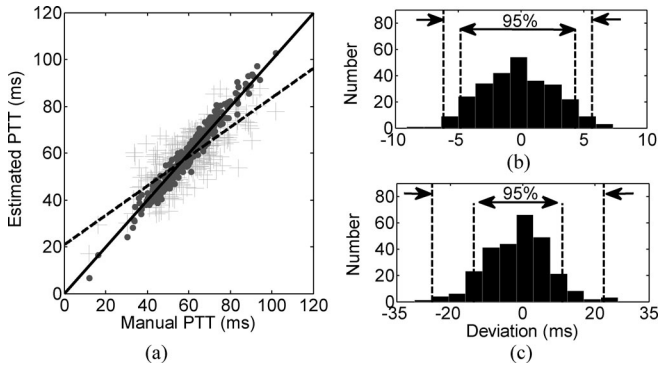

Fig. 5. PTT estimation evaluation. (a) Estimated PTT using DaT method (shown with "+") and JEKF method (shown with ".") vs. the manual PTT determined by the cardiologist. The least square error regression lines are also shown (JEKF: solid; DaT: dashed). (b) Histograms of deviations between the markings of the proposed JEKF algorithm compared to the manually measured PTT indices. (c) Histograms of deviations between the markings of the DaT technique compared to the manually measured PTT indices. The 95% and 99% confidence intervals are shown with vertical dashed lines.

measured indices after joint filtering remains in a small error bound, yielding smaller confidence intervals for the error distributions. This illustrates the ability of the joint framework for removing artifacts while preserving important diagnostic features and relevant clinical information of the filtered data.

B. CV Signal Segmentation and PTT Estimation

To test the proposed algorithm for PTT estimation, we have used the same ECG–ABP segments that were used to evaluate the QT and blood pressure estimates (see Section III-A). For performance comparison, we have also examined the traditional derivative and threshold method (DaT) [49]–[52]. To assess the accuracy of estimations with real clinical PTT parameter, we asked two experienced cardiologists from Tehran Heart Center to annotate our data. The first annotator provided complete annotations for all patients/beats. However, the second annotator delineated only the first few beats from each patient. For the beats that we had both annotators' delineation, interobserver standard deviation was less than 4 ms.

In Fig. 5(a), we plot the estimated PTTs versus manual PTTs for both methods. We also show the least square error linear regression for the scattered data. We observe a high degree of correlation between the PTT estimations from JEKF and real PTT ($r = 0.98$, $p < 0.001$, regression line: $Y = 0.998X + 1.71 \times 10^{-8}$), while PTTs measured by the DaT algorithm show a significant difference compared to the manual standard ($r = 0.76$, $p < 0.001$, regression line: $Y = 0.628X + 20.77$). To assess the accuracy of the PTT estimation, in Fig. 5(b) and (c), we present the histogram of deviations between the markings of the JEKF algorithm (panel b) and the DaT method (panel c) compared to the manually measured PTT by the experienced cardiologist. It can be seen that the JEKF structure provides a reliable PTT estimation by first, providing a noise free set of observation signals and second, measuring the PTT based on Gaussian descriptors, and therefore gives PTT values very close to real indices ($\Delta\text{PTT}_{\text{JEKF}}$: mean $\pm$ std $= -0.26 \pm 2.93$ ms; $\Delta\text{PTT}_{\text{DaT}}$: mean $\pm$ std $= -1.32 \pm 8.84$ ms). The results demonstrate that JEKF deviations have a normal distribution and the error is not considerable (99-percentile: 5.92 ms, 95-percentile: 4.57 ms). Note that the 95% region is less than 6 ms, which is better than interobserver differences in annotating QT intervals [53]. Moreover, the error bounds are smaller than the previously reported 9–10 ms variation of PTT in normal subjects [33], [54]. Our results suggest that the proposed automated method has an acceptable accuracy close to the experts' measurements for clinical evaluations.

IV. Discussion and Conclusion

In the light of extensive studies [10], [11], [13]–[20], [22], [28]–[31], [43], [44], [55] toward model-based ECG processing demonstrating an association between temporal characteristics of heart cycle and the spatial morphological variations, the accurate modeling of the cardiac electromechanical dynamism may hold promise as an approach to facilitate data analysis and information extraction. This study aims to investigate the utility of a minimal order joint model-to-model phase and co-occurrence information of a coupled pair of ECG–ABP signals, with applications to filtering and segmentation. The advantage of joint modeling is that it can provide a means of joint filtering, and the temporal information of the waveforms could be derived using the filtered signals. Additionally, due to the dynamic nature of the model, the filter can adapt with different spectral shapes and temporal nonstationarities. Therefore, we hypothesized that 1) the model should be able to provide a robust filtering of noisy observations, with performances compared to or better than the current benchmark method, and 2) the Kalman filter estimations may be used to determine time-point-based features such as PTT.

The designed filter was applied to standard multiparameter databases. Compared to benchmark denoising methods, the proposed JEKF and JEKS provides a larger SNR improvement, especially in lower input SNRs, where the original signal is lost in noise (8.40 dB $\leq$ SNR improvement $\leq$ 23.19 dB). In addition, we showed that the ST improvement for the joint methods is in the same range with the signal improvement, illustrating the ability of the joint filter to preserve low amplitude components. Furthermore, assessment of the filtering performance using clinically relevant features showed that the method has a minimum effect on diagnostic features of the signals (ΔQT: mean $\pm$ std $= 2.2 \pm 6.1$ ms; ΔSBP: mean $\pm$ std $= 2.3 \pm 1.9$ mmHg; ΔDBP: mean $\pm$ std $= 1.9 \pm 1.4$ mmHg). Finally, the model was shown to provide a robust PTT estimation ($r = 0.98$, $p < 0.001$, mean $\pm$ std of error $= -0.26 \pm 2.93$ ms).

This study is the *first* to provide a comprehensive and systematic approach into exploring the ability to model a pair of CV signals to provide robust estimations and determine correlated transmission time using the KF outputs. Specifically, the main contributions of this work are 1) the proposal of a minima order Kalman-based joint filtering algorithm to provide robust estimations of the input noisy measurements of coupled CV signals at once; and 2) PTT estimation from coupled ECG–ABP signals using the EKF estimations. It should be noted that the

phase-derived interaction introduced in this study is a first attempt to define a minimal joint representation to relate the time cycle of the whole pulsatile events in ECG and ABP, and would be sufficient to achieve the specific aims of this study. However, a more elegant approach is to consider more comprehensive interactions where the occurrence of each event in ECG may be correlated to the onset or offset of another event in ABP signal. This requires a more elaborate analysis of the electromechanical modulations between CV signals.

Since the proposed framework is based upon dynamical GMMs, the model is versatile enough to be applied to a wide variety of bandlimited quasi-periodic signals that spontaneously originate from the cardiac pulsation, either reflecting the electrical conduction of the heart (such as body surface ECG or intracardiac electrograms) or the modulated mechanical response to the propagation of this activity (such as CV pressure signals including ABP, CVP, PAP, PPG, and optical reflectance or transmittance signals commonly used in pulse oximetry).

Our proposed framework is built upon EKF and EKS structures for their simplicity and improved numerical stability over other Bayesian filters. However, other generalizations of the KF recursions such as the sigma-point KF [56], [57] and particle filters [58], [59] can be used in the same manner for highly nonlinear and non-Gaussian noise scenarios. It should be noted that the use of additive noise terms η_{ECG} and η_{ABP} that account for the effects of the mismatch with a true pair of ECG–ABP signals gives more flexibility to the Kalman filter, and prevents it from converging to undesired limit cycles [60].

The current framework implementation uses the estimated phase signal to find the zero crossing for PTT estimation; however, it is possible to incorporate the variables of the Gaussian inside the state vectors and assign autoregressive dynamics to the Gaussian parameters, as investigated in [43], to obtain direct estimations from the KF. This requires introducing a more complex model with more state variables and new process noise components, which leads to a new model with increased dimensions.

From an arrhythmia detection perspective, it is possible to use the methodology proposed in [13] and employ the signal fidelity to determine rhythm disturbances. This may have important clinical implications to the detection of erroneous hypertensive or hypotensive episodes, and to identifying the electromechanical modulation of CV signals during abnormal events such as tachyarrhythmic events or pulseless electrical activity [13].

In conclusion, we presented a minimal order joint model and validated its utility to address important clinical problems, including filtering and correlated feature extraction. Our results demonstrate that the proposed algorithm provides high fidelity estimations of coupled CV signals, with which accurate PTT estimations may be obtained.

ACKNOWLEDGMENT

The authors would like to thank Dr. G. D. Clifford and Dr. S. Sadeghian for their valuable feedbacks and the Tehran Heart Center. They would also like to thank the anonymous reviewers for their helpful comments.

REFERENCES

[1] M. D. Cheitlin, M. Sokolow, and M. B. Mcllroy, *Clinical Cardiology*. Norwalk, CT, USA: Appleton & Lange, 1993.
[2] R. Virmani, *Cardiovascular Pathology*. New York, NY, USA: Elsevier, 2001.
[3] L. Rovere, "Methods to assess baroreflex sensitivity as a measure of the activity of the autonomic nervous system," in *Advances in Noninvasive Electrocardiograph Monitoring Techniques*, H.-H. Osterhues, V. Hombach, and A. J. Moss, Eds. Norwell, MA, USA: Kluwer, 2000.
[4] M. Appel, R. Berger, J. P. Saul, J. Smith, and R. Cohen, "Beat to beat variability in cardiovascular variables: Noise or music," *J. Amer. Coll. Cardiol.*, vol. 14, no. 5, pp. 1139–1148, 1989.
[5] R. Kitney, T. Fulton, A. McDonald, and D. Linkens, "Transient interactions between blood pressure, respiration and heart rate in man," *J. Biomed. Eng.*, vol. 7, no. 3, pp. 217–224, 1985.
[6] A. Rozanski, J. A. Blumenthal, and J. Kaplan, "Impact of psychological factors on the pathogenesis of cardiovascular disease and implications for therapy," *Circulation*, vol. 99, pp. 2192–2217, 1999.
[7] K. F. Harris and K. A. Matthews, "Interactions between autonomic nervous system activity and endothelial function: A model for the development of cardiovascular disease," *Psychosom. Med.*, vol. 66, pp. 153–164, 2004.
[8] D. Dubin, *Rapid Interpretation of EKG's*. Tampa, FL, USA: Cover, 2000.
[9] M. J. Kern, M. J. Lim, and J. A. Goldstein, Eds., *Hemodynamic Rounds: Interpretation of Cardiac Pathophysiology From Pressure Waveform Analysis*. New York, NY, USA: Wiley, 2009.
[10] G. D. Clifford and P. E. McSharry, "Generating 24-hour ECG, BP and respiratory signals with realistic linear and nonlinear clinical characteristics using a nonlinear model," *Comput. Cardiol.*, vol. 31, pp. 709–712, 2004.
[11] G. D. Clifford and P. E. McSharry, "A nonlinear artificial model for generating realistic correlated ECG, BP and respiration," in *Proc. 17th Int. EURASIP Biosignal Conf.*, Brno, Czech Republic, 2004, pp. 358–360.
[12] J. McNames and M. Aboy, "Statistical modeling of cardiovascular signals and parameter estimation based on the extended Kalman filter," *IEEE Trans. Biomed. Eng.*, vol. 55, no. 1, pp. 119–129, Jan. 2008.
[13] O. Sayadi and M. B. Shamsollahi, "Life-threatening arrhythmia verification in ICU patients using the joint cardiovascular dynamical model and a Bayesian filter," *IEEE Trans. Biomed. Eng.*, vol. 58, no. 10, pp. 2748–2757, Oct. 2011.
[14] O. Sayadi and M. B. Shamsollahi, "A combined dynamical sequential network for generating coupled cardiovascular signals with different beat types," in *Proc. 3rd Int. Symp. Appl. Biomed. Commun. Technol.*, Rome, Italy, 2010, pp. 1–5.
[15] G. D. Clifford and R. Sameni, "An artificial multi-channel model for generating abnormal electrocardiographic rhythms," in *Proc. Comput. Cardiol.*, 2008, pp. 773–776.
[16] G. D. Clifford, S. Nemati, and R. Sameni, "An artificial vector model for generating abnormal electrocardiographic rhythms," *Physiol. Meas.*, vol. 31, no. 5, pp. 595–609, May 2010.
[17] P. E. McSharry, G. D. Clifford, L. Tarassenko, and L. A. Smith, "A dynamic model for generating synthetic electrocardiogram signals," *IEEE Trans. Biomed. Eng.*, vol. 50, no. 3, pp. 289–294, Mar. 2003.
[18] R. Sameni, M. B. Shamsollahi, C. Jutten, and M. Babaie-Zadeh, "Filtering noisy ECG signals using the extended Kalman filter based on a modified dynamic ECG model," in *Proc. 32nd Annu. Int. Conf. Comput. Cardiol.*, Lyon, France, Sep. 25–28, 2005, pp. 1017–1020.
[19] R. Sameni, M. B. Shamsollahi, C. Jutten, and G. D. Clifford, "A nonlinear Bayesian filtering framework for ECG denoising," *IEEE Trans. Biomed. Eng.*, vol. 54, no. 12, pp. 2172–2185, Dec. 2007.
[20] O. Sayadi, M. B. Shamsollahi, and G. D. Clifford, "Robust detection of premature ventricular contractions using a wave-based Bayesian framework," *IEEE Trans. Biomed. Eng.*, vol. 57, no. 2, pp. 353–362, Feb. 2010.
[21] G. Baselli, S. Cerutti, S. Civardi, D. Liberati, F. Lombardi, A. Malliani, and M. Pagani, "Spectral and cross-spectral analysis of heart rate and arterial blood pressure variability signals," *Comput. Biomed. Res.*, vol. 19, pp. 520–534, 1986.
[22] R. Sameni, G. D. Clifford, C. Jutten, and M. B. Shamsollahi, "Multichannel ECG and noise modeling: Application to maternal and fetal ECG signals," *EURASIP J. Adv. Signal Process.*, vol. 2007, pp. 043407-1–043407-14, 2007.
[23] M. Malik and A. J. Camm, *Heart Rate Variability*. Armonk, NY, USA: Futura, 1995.

[24] G. D. Clifford, F. Azuaje, and P. E. McSharry, Eds., *Advanced Methods and Tools for ECG Data Analysis*. Norwood, MA, USA: Artech House, 2006.
[25] S. M. Kay, *Fundamentals of Statistical Signal Processing: Estimation Theory*. Englewood Cliffs, NJ, USA: Prentice-Hall, 1993.
[26] S. Haykin, Ed., *Kalman Filtering and Neural Networks*. New York, NY, USA: Wiley, 2001.
[27] D. Simon, Ed., *Optimal State Estimation*. New York, NY, USA: Wiley, 2006.
[28] G. D. Clifford, A. Shoeb, P. E. McSharry, and B. A. Janz, "Model-based filtering, compression and classification of the ECG," *Int. J. Bioelectromagn.*, vol. 7, pp. 158–161, 2005.
[29] G. D. Clifford and M. Villarroel, "Model-based determination of QT intervals," in *Proc. Comput. Cardiol.*, 2006, pp. 357–360.
[30] O. Sayadi and M. B. Shamsollahi, "A model-based Bayesian framework for ECG beat segmentation," *Physiol. Meas.*, vol. 30, pp. 335–352, 2009.
[31] O. Sayadi and M. B. Shamsollahi, "Model-based ECG fiducial points extraction using a modified extended Kalman filter structure," in *Proc. 1st Int. Symp. Appl. Biomed. Commun. Technol.*, Aalborg, Denmark, 2008, pp. 1–5.
[32] M. J. Drinnan, J. Allen, and A. Murray, "Relation between heart rate and pulse transit time during paced respiration," *Physiol. Meas.*, vol. 22, pp. 425–432, 2001.
[33] R. P. Smith, J. Argod, J. Pépin, and P. A. Lévy, "Pulse transit time: An appraisal of potential clinical applications," *Thorax*, vol. 54, pp. 452–458, 1999.
[34] S. Greenwald, E. Olofsen, and A. Dahan, "Pulse transit time (PTT) reflects changes in anesthetic state during sevolfurane/N_2O anesthesia," *Anesthesiology*, vol. 96, p. 544, 2002.
[35] G. Sharwood-Smith, J. Bruce, and G. Drummond, "Assessment of pulse transit time to indicate cardiovascular changes during obstetric spinal anaesthesia," *Brit. J. Anaesth.*, vol. 96, pp. 100–105, 2006.
[36] S. Singham, L. Voss, J. Barnard, and J. Sleigh, "Nociceptive and anaesthetic induced changes in pulse transit time during general anaesthesia," *Brit. J. Anaesth.*, vol. 91, pp. 662–666, 2003.
[37] M. C. Kortekaas, S. P. Niehof, M. H. N. van Velzen, E. Galvin, F. Huygen, and R. Stolker, "Pulse transit time as a quick predictor of a successful axillary brachial plexus block," *Acta Anaesthesiol.*, vol. 56, pp. 1228–1233, 2012.
[38] J. R. Stradling, C. Barbour, J. Glennon, B. A. Langford, and J. H. Crosby, "Which aspects of breathing during sleep influence the overnight fall of blood pressure in a community population?" *Thorax*, vol. 55, no. 5, pp. 393–398, May 2000.
[39] The MIMIC Database. (2012). [Online]. Available: http://www.physionet.org/physiobank/database/mimicdb
[40] A. L. Goldberger, L. Amaral, L. Glass, J. M. Hausdorff, P. Ivanov, R. G. Mark, J. E. Mietus, G. B. Moody, C.-K. Peng, and H. E. Stanley, "PhysioBank, PhysioToolkit, and PhysioNet: Components of a new research resource for complex physiologic signals," *Circulation*, vol. 101, pp. e215–e220, 2000.
[41] The MIT-BIH Noise Stress Test Database. (2012). [Online]. Available: http://www.physionet.org/physiobank/database/nstdb
[42] P. A. Laizzo, *Handbook of Cardiac Anatomy, Physiology, and Devices*. New York, NY, USA: Springer, 2009.
[43] O. Sayadi and M. B. Shamsollahi, "ECG denoising and compression using a modified extended Kalman filter structure," *IEEE Trans. Biomed. Eng.*, vol. 55, no. 9, pp. 2240–2248, Sep. 2008.
[44] O. Sayadi, R. Sameni, and M. B. Shamsollahi, "ECG denoising using parameters of ECG dynamical model as the states of an extended Kalman filter," in *Proc. Annu. Int. Conf. IEEE Eng. Med. Biol. Soc.*, Lyon, France, 2007, pp. 2548–2551.
[45] Q. Li, R. G. Mark, and G. D. Clifford, "Artificial arterial blood pressure artifact models and an evaluation of a robust blood pressure and heart rate estimator," *BioMed. Eng. OnLine*, vol. 8, no. 13, pp. 1–15, 2009.
[46] Y. Zigel, A. Cohen, and A. Katz, "The weighted diagnostic distortion measure for ECG signal compression," *IEEE Trans. Biomed. Eng.*, vol. 47, no. 11, pp. 1422–1430, Nov. 2000.
[47] C. Li, C. Zheng, and C. Tai, "Detection of ECG characteristic points using wavelet transforms," *IEEE Trans. Biomed. Eng.*, vol. 42, no. 1, pp. 21–28, Jan. 1995.
[48] F. Gritzali, G. Frangakis, and G. Papakonstantinou, "Detection of the P and T waves in an ECG," *Comput. Biomed. Res.*, vol. 22, pp. 83–91, 1989.
[49] D. Barschdorff, M. Erig, and E. Trowitzsch, "Noninvasive continuous blood pressure determination," in *Proc. XVI IMEKO World Congr.*, Wien, Austria, 2000, pp. 1–5.
[50] Y. Yoon, J. H. Cho, and G. Yoon, "Non-constrained blood pressure monitoring using ECG and PPG for personal healthcare," *J. Med. Syst*, vol. 33, no. 4, pp. 261–266, 2009.
[51] A. V. Deshmane, "False arrhythmia alarm suppression using ECG, ABP, and photoplethysmogram," M.S. thesis, Massachusetts Inst. Technol., Dept. Electr. Eng. Comput. Sci., Cambridge, MA, USA, 2009.
[52] S. Ahmad, S. Chen, K. Soueidan, I. Batkin, M. Bolic, H. Dajani, and V. Groza, "Electrogram-assisted blood pressure estimation," *IEEE Trans. Biomed. Eng.*, vol. 59, no. 3, pp. 608–618, Mar. 2012.
[53] G. B. Moody, H. Koch, and U. Steinhoff, "The physionet/computers in cardiology challenge 2006: QT interval measurement," in *Proc. Comput. Cardiol.*, 2006, pp. 313–316.
[54] M. Sigtermans, J. Looijestijn, E. Olofsen, and A. Dahan, "Pulse transit time (PTT) measurements during laparoscopic and open abdominal surgery: A pilot study in ASA I-II female patients," *Open Anesthesiol. J.*, vol. 2, pp. 20–25, 2008.
[55] R. Vullings, B. de Vries, and J. W. Bergmans, "An adaptive Kalman filter for ECG signal enhancement," *IEEE Trans. Biomed. Eng.*, vol. 58, no. 4, pp. 1094–1103, Apr. 2011.
[56] A. Gelb, *Applied Optimal Estimation*. Cambridge, MA, USA: MIT Press, 1974.
[57] E. Wan and R. V. D. Merwe, *The Unscented Kalman Filter*. New York, NY, USA: Wiley, 2001.
[58] P. M. Djurić, J. H. Kotecha, J. Zhang, Y. Huang, T. Ghirmai, M. F. Bugallo, and J. Míguez, "Particle filtering," *IEEE Signal Process. Mag.*, vol. 20, no. 5, pp. 19–38, Sep. 2003.
[59] R. V. D. Merwe, "Sigma-Point Kalman filters for probabilistic inference in dynamic state-space models," Ph.D. dissertation, OGI School Sci. Eng., Oregon Health Sci. Univ., Hillsboro, OR, USA, Apr. 2004.
[60] G. B. Moody and R. G. Mark, "QRS morphology representation and noise estimation using the Karhunen–Loève transform," in *Proc. Comput. Cardiol.*, Jerusalem, Israel, 1989, pp. 269–272.

Omid Sayadi (S'06–M'12) received the M.Sc. and Ph.D. degrees in Electrical Engineering, both with highest honor from Sharif University of Technology, Tehran, Iran, in 2007 and 2010, respectively.

He is currently an American Heart Association Postdoctoral Fellow at the Harvard Medical School, Boston, MA, USA, where he is also a member of the Cardiovascular Research Center, Massachusetts General Hospital.

Dr. Sayadi has received more than 10 awards, including the Outstanding Graduation Award in Biomedical Engineering, Iran Telecommunication Research Center Award, Highest Distinction Award in Bioelectrics, Exceptional Talents Center Research Award, Outstanding Ph.D. Graduation Award in Biomedical Engineering, Departmental Full Research Scholarship, Excellence in Teaching, American Heart Association Founders Affiliate Postdoctoral Fellowship and most recently the Kenneth M. Rosen Fellowship in Cardiac Pacing and Electrophysiology, awarded by the Heart Rhythm Society. His research interests include biomedical signal processing, application of Kalman filters and wavelets in biosignals, and preventive technologies to treat cardiac tachyarrhythmias.

Mohammad Bagher Shamsollahi (M'02) received the B.Sc. degree in electrical engineering from Tehran University, Tehran, Iran, in 1988, the M.Sc. degree in electrical engineering, telecommunications, from the Sharif University of Technology, Tehran, in 1991, and the Ph.D. degree in electrical engineering, biomedical signal processing, from the University of Rennes 1, Rennes, France, in 1997.

He is currently a Professor with the Department of Electrical Engineering, Sharif University of Technology. His research interests include biomedical signal processing, brain–computer interface, and time-scale and time–frequency signal processing.